A Model Study of the Stably Stratified Steady-State Atmospheric Boundary Layer over a Slightly Inclined Terrain

ZBIGNIEW SORBJAN[1]

Geophysical Institute, University of Alaska, Fairbanks, AK 99701

(Manuscript received 9 September 1983, in final form 1 March 1984)

ABSTRACT

A simple, steady-state, numerical model is used to examine the Rossby-number similarity theory of the atmospheric boundary layer over a slightly inclined terrain. The model confirms the similarity predictions. The slope-influenced universal profiles of the wind velocity defects and the stress components are obtained by the model simulation.

1. Introduction

Studies of the stably stratified atmospheric boundary layer (ABL) are not new and have been reported; however, they have not received as much attention in the literature as investigations of its convective counterpart. The first-order closure model of Businger and Arya (1974) and the second-order closure model of Wyngaard (1975) can be mentioned as representative examples of the numerical studies on the stable ABL. Also, the numerical model of Brost and Wyngaard (1975), as well as the analytical models of Mahrt and Schwerdtfeger (1970) and Gutman and Melgarejo (1981) can serve as examples of studies on stably stratified flow over a sloping terrain.

The present paper, although dealing with the same problems, has another aspect, connected with our previous papers on Rossby-number similarity theory of ABL over a slightly inclined terrain (Sorbjan, 1983a,b; hereafter referred to as S83). In these papers, we found the form of the geostrophic drag and heat transfer laws and the form of the similarity functions A, B and C. Moreover, the slope influence on the ABL parameters was predicted by a numerical solution of the resistance laws. All results had a theoretical aspect and were not compared with other investigations.

In our previous papers, we developed a simple diagnostic model of the atmospheric boundary layer to examine the Rossby-number similarity over a sloping terrain. It is important to note that the ABL differs essentially in its structure depending on whether the slope is heated or cooled due to different stability conditions. In the present paper, we limit ourselves to the stable case, where the slope is cooled. The results can simulate the situation where the flow occurs over a mild but permanent slope and is mostly stably stratified, i.e., the Antarctic ABL.

2. The model

The dynamics of the stably stratified boundary layer are governed by a number of physical processes. The nature of some, like intermittency, gravity waves and entrainment through the top of the ABL, is not well understood and will not be considered in our study. Instead, we focus on the effects of gravitationally induced local flow over a slope, caused by the radiative cooling of the surface.

We consider an infinite surface of uniform roughness and temperature distribution, sloped at a small angle ψ to the horizontal (Fig. 1). We also assume that the flow is defined by the dynamic balance between Coriolis, frictional and drainage forces, and expressed in the dimensionless form:

$$\left.\begin{aligned} \frac{d^2X}{dZ^2} + \frac{(sY - \eta H)}{K} &= s\eta_y \\ \frac{d^2}{dZ^2}(sY - \eta H) - \frac{X}{K} &= -\eta_x \end{aligned}\right\}. \tag{1}$$

(All symbols are listed in the Appendix.)

Set (1) follows from dimensionless equations of motion of the form

$$\left.\begin{aligned} \kappa \frac{u'}{u_*} &= \frac{d(sY)}{dZ} + \eta_x Z \\ s\kappa \frac{v'}{u_*} &= \eta \frac{\theta'}{T_*} - \frac{dX}{dZ} + s\eta_y Z \end{aligned}\right\}, \tag{2}$$

derived in S83, where the dimensionless momentum and heat fluxes obey

[1] Permanent affiliation: Institute of Environmental Engineering, Warsaw Polytechnic University, Poland.

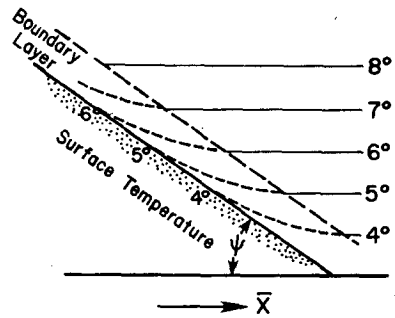

FIG. 1. Idealized distribution of temperature isopleths in the free atmosphere (solid) and in the boundary layer (dashed) during night (the slope in the figure is highly exaggerated).

$$X = K\frac{d}{dZ}\left(\kappa\frac{u}{u_*}\right), \tag{3a}$$

$$Y = K\frac{d}{dZ}\left(\kappa\frac{v}{u_*}\right), \tag{3b}$$

$$H = K\frac{d}{dZ}\left(\frac{\theta'}{T_*}\right), \tag{3c}$$

and H is assumed to be a linear function of height. The primes denote the deviations of the boundary layer parameters from the free atmosphere values:

$$\left.\begin{aligned} u' &= u - G_0\cos\chi \\ v' &= v - G_0\sin\chi \\ \theta' &= \theta - \theta_F \end{aligned}\right\}. \tag{4}$$

The dimensionless components of the thermal wind are defined as

$$\left.\begin{aligned} \eta_x &= \frac{\kappa^2}{f}\frac{dU_g}{dz} = M\cos\phi \\ \eta_y &= \frac{\kappa^2}{f}\frac{dV_g}{dz} = M\sin\phi \end{aligned}\right\}. \tag{5}$$

In the above equations,

$$Z = \frac{z}{L_E},\quad K = \frac{k}{L_E^2 f},\quad L_* = \frac{u_*^2}{\kappa^2\beta T_*},\quad L_E = \frac{\kappa u_*}{f},$$

$$\mu_0 = \frac{L_E}{L_*},\quad T_* = \frac{Q_0}{\kappa u_*},\quad \eta = \frac{\mu_0\psi}{\kappa^2}, \tag{6}$$

where

X, Y	components of the stress vector ($\overline{u'w'}$, $\overline{v'w'}$), nondimensionalized by u_*^2
θ, θ_F	potential temperature in the ABL and in the free atmosphere
u, v	components of the wind velocity
G_0, U_g, V_g	surface geostrophic wind velocity and the components of the geostrophic wind vector
χ	angle between the x-axis and the geostrophic wind vector
u_*	friction velocity
β	buoyancy parameter
κ	von Kàrmàn constant
f, s	modulus and sign of the Coriolis parameter
k	eddy diffusivity
Q_0	surface heat flux [$=c_p\rho\overline{w'u'}$]
ψ	slope inclination
z	vertical axis of the Cartesian coordinate, normal to the earth's surface; x-axis is oriented down the slope.

The temperature deviation θ' from the free atmosphere value, which is negative in stable conditions, produces a height-dependent, additional pressure gradient (additional component of the thermal wind, named here "local thermal wind" in contrast to "synoptic thermal wind").

Rewriting the set (2) in the form below displays the balance of the acting forces:

$$\frac{d}{dZ}[X, sY] - \mathbf{k}\cdot\left[\kappa\frac{u'}{u_*} - \eta_x Z,\ s\kappa\frac{v'}{u_*} - \left(s\eta_y Z + \eta\frac{\theta'}{T_*}\right)\right] = 0. \tag{7}$$

We can see clearly that the corresponding additional component of the thermal wind, acting along the y-axis, is parallel to the contour lines of the terrain and is proportional to the strength of the inversion and to the slope of the ground ($\mathbf{k}$ is the unit vector of the z-axis).

We assume a steady state and therefore, all ABL parameters to be independent of time. This situation can be established by balancing the cooling through the turbulent heat flux divergence, and the warming through mean advection. It can occur, for example, over Antarctica, where observations show small diurnal variations of the temperature, especially during the polar night (Wendler and Kodama, 1983).

In a steady state, the turbulence is in local equilibrium, since the turbulent time scale $\tau_t = z_T/u_*$ (z_T is the height of the ABL) is much smaller than the time scale of the temperature changes. As a result, the turbulent structure represented in our model by the turbulent heat flux, the eddy diffusivity and the height of the boundary layer, should depend only on the local mean conditions and can be described in a simple, universal form. On the basis of this remark, we close (1), (2) in the following way:

$$\left.\begin{aligned} H &= H_0\left(1 - \frac{Z}{Z_T}\right)^p \\ K &= \frac{Z}{1 + \beta_0\mu_0 Z}\left(1 - \frac{Z}{Z_T}\right)^q \\ Z_T &= c\mu_0^r,\ \mu_0 \gg 1 \end{aligned}\right\}, \tag{8}$$

where H_0 is the dimensionless surface heat flux.

The formula for the dimensionless heat flux H is independent of synoptic baroclinicity, which is assumed to be weak. We also assume that because the slope is small, H is independent of slope characteristics (S83). To describe the vertical distribution of H, we employ the frequently used exponential formula. The value of p is not as certain. The power p was reported to be approximately 1.5 by Yokoyama *et al.* (1979). However, from the plot presented in their paper, it appears that p can be estimated equal to 1 as well. The value 1 was accepted in S83 to derive the similarity functions A, B and C.

The expression for the eddy diffusivity K was proposed by Brost and Wyngaard (1978). In the surface layer, the expression follows the results of Businger *et al.* (1971) with $\beta_0 = 4.7$. The value of q was suggested to be equal to 1.5. Brost and Wyngaard (1978) also reported a good agreement of this formula with the eddy diffusivity profiles, obtained over the sloping terrain in Antarctica (Kuhn *et al.*, 1977).

The height of the stable boundary layer is described by the formula obtained from the similarity prediction of Zilitinkevich (1972, 1975), with $r = -0.5$. We assumed that the ABL height is constant along the slope and independent of the slope. This is a simplification, since in a real situation we should expect z_T to be dependent on the orientation and the magnitude of the slope (Brost and Wyngaard, 1978). We set the constant $c = 0.8$. Wyngaard (1975) obtained $c = 0.35$, while Brost and Wyngaard (1978) found $c = 0.63$ and Businger and Arya (1974), $c = 1.14$.

The lower boundary condition for the set (1), (2) can be written in the form:

FOR $Z = Z_0$

$$\left.\begin{aligned} &X = \cos\delta, \quad Y = \sin\delta, \quad H = H_0 = \frac{1}{\alpha_H^0} \\ &\kappa\frac{u'}{u_*} = -\kappa\frac{\cos\chi}{c_g}, \quad \kappa\frac{v'}{u_*} = -\kappa\frac{\sin\chi}{c_g}, \quad \frac{\theta'}{T_*} = \frac{\theta_0'}{T_*} \end{aligned}\right\}, \tag{9}$$

where δ is the angle between the x-axis and the surface stress vector and c_g is the geostrophic drag coefficient ($c_g = u_*/G$). Ignoring the entrainment effects, we assume that at the top of the boundary layer:

FOR $Z = Z_T$

$$X = 0, \quad Y = 0, \quad H = 0, \quad \frac{\theta'}{T_*} = 0. \tag{10}$$

If α is the angle between the surface stress vector and the geostrophic wind vector, then $\alpha = \chi - \delta$, independent of the hemisphere (Fig. 2). The set (1) is independent of the hemisphere, since it can be considered with respect to the products sY, $s\delta$ and $s\phi$.

The ABL characteristics $\kappa u'/u_*$, $\kappa v'/u_*$, X and Y can now be obtained through the numerical integration

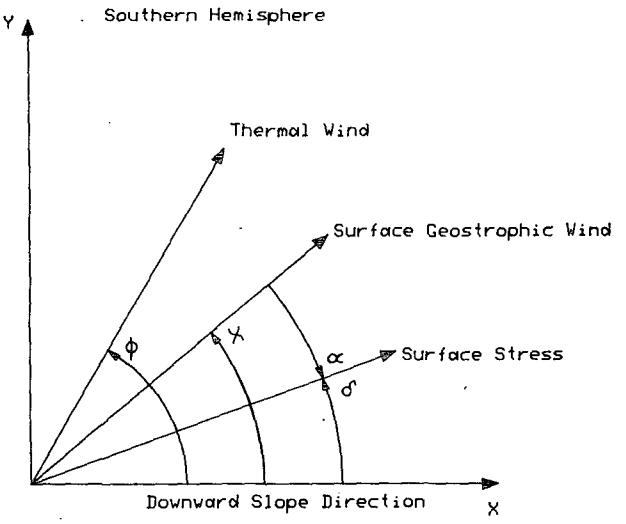

FIG. 2. The orientation of the angles α, δ, χ and ϕ.

of the governing equations. Each of them depend on the six governing parameters ψ, μ_0, δ, η_x, η_y and s.

The surface value θ_0'/T_* is calculated integrating the third equation in (3) from the bottom to the top of the boundary layer:

$$-\frac{\theta_0'}{T_*} = \int_{Z_0}^{Z_T}\frac{H}{K}\,dZ = \frac{1}{\alpha_H^0}\ln\frac{Z_T}{Z_0} + \frac{\beta_0\mu_0}{\alpha_H^0}(Z_T - Z_0), \tag{11}$$

where we assumed that $p = q$ (to satisfy the surface similarity) and that θ' vanishes on the top of the ABL. We set $p = 1$, as in S83.

It should be mentioned that the temperature profile is sensitive to the specification of p and q. From (3a) and (8a, b), it follows that for $p < q$, a gradient of Θ'/T_* blows up at the boundary layer top. For $p = q$, singularity is never realized.

From (2) and (9) we have

$$c_g = \kappa\left\{\left[\left\{\left.\frac{dX}{dZ}\right|_{Z_0} - \eta\frac{\theta_0'}{T_*}\right\}^2 + \left\{\left.\frac{dY}{dZ}\right|_{Z_0}\right\}^2\right]\right\}^{-1/2}, \tag{12}$$

$$\chi = \arctan\left\{-\frac{\left[\left.\frac{dX}{dZ}\right|_{Z_0} - \eta\frac{\theta_0'}{T_*}\right]}{\left.\frac{dY}{dZ}\right|_{Z_0}}\right\}. \tag{13}$$

The similarity functions of the resistance laws over a sloping terrain can be expressed in the form obtained in S83:

$$\left.\begin{aligned} A_s &= s\left.\frac{dY}{dZ}\right|_{Z_0} - \cos\delta\ln(\kappa Z_0) \\ B_s &= -\left.\frac{dX}{dZ}\right|_{Z_0} - \left(s\sin\delta - \frac{\eta}{\alpha_H^0}\right)\ln(\kappa Z_0) \\ C_s &= \alpha_H^0\frac{\theta_0'}{T_*} - \ln(\kappa Z_0) \end{aligned}\right\}. \tag{14}$$

It is suitable to introduce the external stability parameter $\sigma = -\beta\theta'_0/(Gf)$, which can be also expressed as

$$\sigma = -\frac{\theta'_0}{T_*}\frac{c_g}{\kappa^3}\mu_0. \tag{15}$$

The external stability parameter σ is available from the synoptic information.

The numerical algorithm, employed for the solution of the governing equations (1), is similar to that described in detail by du Vachat and Musson-Genon (1982). The function θ'/T_* was obtained by numerical integration of Eq. (3c), differentiated with respect to Z, with the boundary conditions (9) and (10).

3. The results

In this section, the results of the model simulation are presented. The discussion is divided into three subsections. In the first, we examine the horizontal version of the model. The flow over a sloping terrain is discussed in the second subsection. Finally, in the third subsection, we discuss the parametrization of the stable boundary layer over a sloping terrain, in terms of the Rossby-number similarity theory.

a. Horizontal surface

First, we shall examine our model for the horizontal case ($\psi = 0$). The agreement of the model prediction with the available data should be a good basis for the further investigations.

The model calculations were done for $\mu_0 = 4$, 25, 50 and 75, for two values of the roughness parameter $Z_0 = 10^{-4}$, 10^{-5}, for $\eta_x = \eta_y = 0$ and for the Southern Hemisphere, $s = -1$. It should be noted that results valid for the Northern Hemisphere can be easily obtained from the plots presented in our paper by changing the sign of the angle δ and of the y-component of all profiles.

The model is based on two main assumptions connected with the eddy diffusivity and turbulent heat flux distribution. Formally, the turbulent terms in the governing equations could be expressed in terms of the "1.5-order-closure" scheme, based on K-theory, and on the turbulent kinetic energy (TKE) equation. However, for the sake of simplicity, instead of the TKE equation, we have employed available empirical information: 1) the turbulent heat flux in the stable boundary layer is a linear function of height, 2) in the surface layer the temperature gradient is log-linear, and 3) the integral of H/K is defined by the similarity function C [Eqs. (11), (14)], given from measurements (Fig. 6). This leads to the accepted formula for K. The eddy diffusivity profiles, for different stability parameters μ_0, are shown in Fig. 3. For $\mu_0 = 4$ and $\mu_0 = 50$, the K distribution is compared with the profiles obtained by Brost and Wyngaard (1978) and by Businger and Arya (1974). The maximum values of K, in our model, exceed the maximum values obtained in the first paper and are smaller than those obtained in the second one.

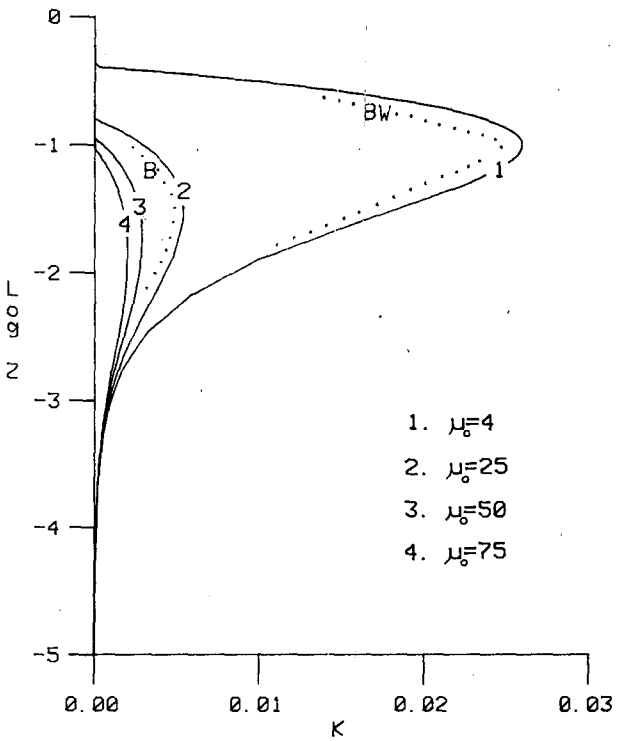

FIG. 3. The eddy diffusivity distribution for different stabilities. BW, profile obtained by Brost and Wyngaard (1978), for $h/L_* = 2$ and $h/L_E = 0.5$ ($\mu_0 = 4$), B, profile obtained by Businger and Arya (1974), $\mu_0 = 50$.

Figure 4 shows the vertical distribution of the dimensionless temperature defect θ'/T_*. Within the surface layer, the temperature defect is logarithmic. The bulk curvature, defined as in André and Mahrt (1982), is positive. According to these authors, the positive curvature is frequently found in the stable boundary layer dominated by turbulence; this agrees with our study.

The surface value of the temperature defect defines the third similarity function C in Eq. (14). The function C, as well as functions A and B, are shown in Fig. 5. All similarity functions are compared with the results obtained by Arya (1975) and based on Wangara data.

In Fig. 6, the cross-isobar angle α and the geostrophic drag coefficient c_g are compared with the results of Arya (1975). The good agreement found in Figs. 5 and 6 is encouraging for the investigations of the sloping terrain case.

b. Slightly inclined terrain

The effects of a sloping terrain extending over hundreds of kilometers refer mainly to the deformation of the wind hodographs and the phenomenon known as the low-level jet (e.g., Lettau, 1983).

The slope-influenced hodographs of the dimension-

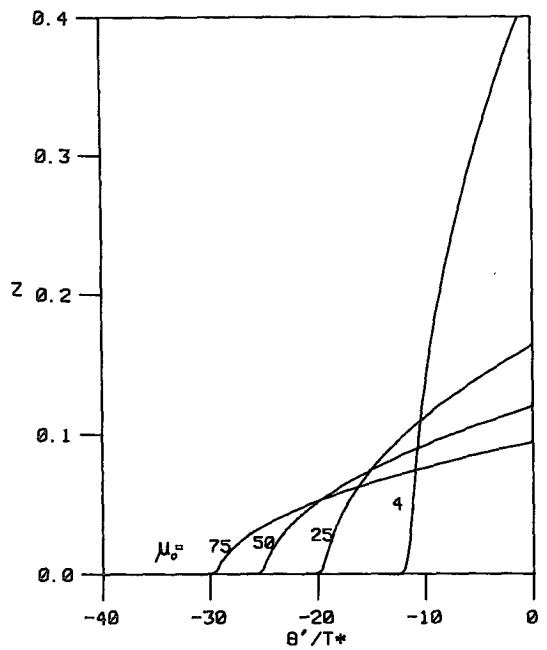

FIG. 4. The dimensionless temperature defects for different stabilities.

less wind velocity defects $\kappa u'/u_*$, $\kappa v'/u_*$, obtained from the model, are shown in Fig. 7 for two stabilities $\mu_0 = 4$ and 50. Here and throughout Section 3b, the slope $\psi = 0.003$ was assumed. From Fig. 7 it is apparent that the influence of the slope increases with the stability. This is because the dimensionless inversion strength θ_0'/T_* is proportional to μ_0 [Eq. (11)]. In Fig. 7, the x-axis is parallel to the downward slope direction. The numbers next to every hodograph mark the angle δ between the x-axis and the surface stress vector. The hodographs for $\mu_0 = 4$ resemble classical Ekman spirals, since the term θ'/T_* in Eq. (7) is small. The hodographs obtained for $\mu_0 = 50$ are less regular. Between $\delta = 315°$ and 0°, a deflection to the right is obtained. It can be seen from the figure that for $0° \leqslant \delta \leqslant 45°$, there is a very small change in wind direction with height. Similar hodographs were obtained by Lettau and Riordan (1977) and Kuhn *et al.* (1977) for the flow at Plateau Station, eastern Antarctica.

The cross-isobar angle α exceeds its horizontal case values for $45° \leqslant \delta \leqslant 225°$, but is smaller in the range $225° \leqslant \delta \leqslant 45°$ (Fig. 8). In Fig. 8, the slope-induced changes of the geostrophic drag coefficient are also shown.

In Figs. 9 and 10, the similarity profiles of X, Y and $\kappa u'/u_*$, $\kappa v'/u_*$ are displayed. The x-axis on the plots is parallel to the surface stress vector. The figures show the substantial influence of the slope orientation.

The dimensionless wind velocity modulus is shown in Fig. 11 for $\mu_0 = 50$ and for different angles δ. It can be seen that the wind became supergeostrophic only for $0° \leqslant \delta \leqslant 180°$ (opposite on the Northern Hemisphere). The heights of the maximum winds are smaller than for the horizontal case.

The significant shear close to the top of the ABL can lead to two effects that have not been considered in our simple model.

The first is the entrainment effect. The entrainment

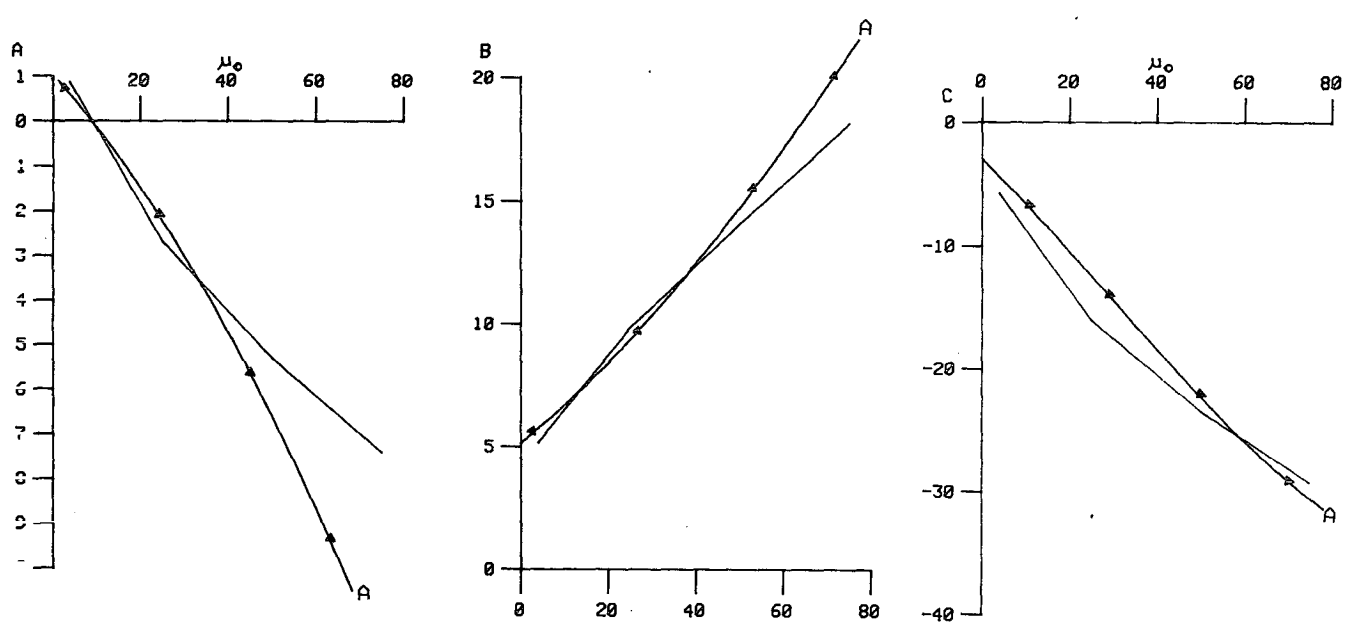

FIG. 5. The comparison of the similarity functions A, B and C calculated from the present model (solid lines) with those obtained by Arya (1975) from the Wangara data (marked lines).

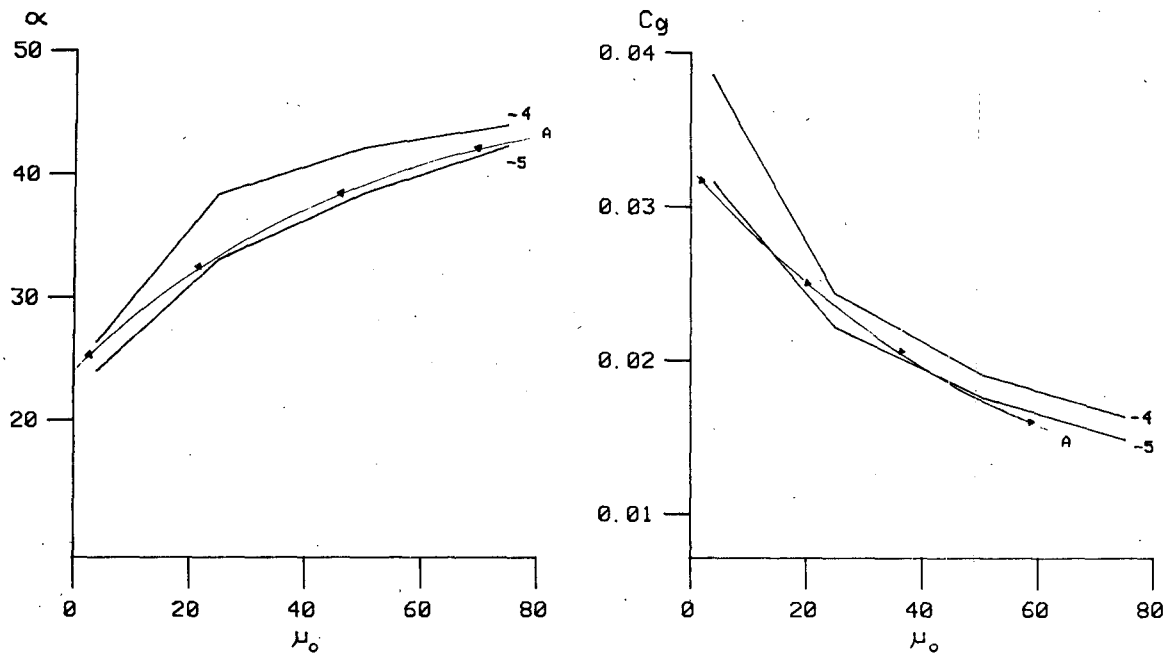

FIG. 6. The comparison of the cross-isobar angle α and the geostrophic drag coefficient c_g, calculated from the model for $\log Z_0 = -4$ and -5, with those obtained by Arya (1975) from the Wangara data (marked lines, Ro = 10^7).

incorporates warmer and slower air from the free atmosphere into the cold air layer next to the ground. It tends to decrease the intensity of the katabatic flow. The dimensionless momentum flux due to entrainment is usually approximated as $E\Delta U$, where E is the dimensionless entrainment velocity and ΔU is the dimensionless strength of the supergeostrophic flow. To estimate the effect of entrainment, we should compare the momentum flux on the top of the ABL with the buoyancy term, which generates the flow. From the integrated form of the second equation in (2), it follows that the momentum flux due to entrainment is unimportant, if $E\Delta U/\eta/Z_T \ll \theta_0'/T_*$. For the typical values of the parameters ($\Delta U \approx 25$, $\eta \approx 1$, $Z_T \approx 0.1$, $\theta_0'/T_* \approx 25$) and for $E \approx 10^{-2}$ (Turner, 1973), we find that the above condition is satisfied in our model. Since the entrainment vanishes with increasing stability, which corresponds to decreasing turbulence, our model is valid only for a certain range of the stability parameter μ_0, in which entrainment can be omitted

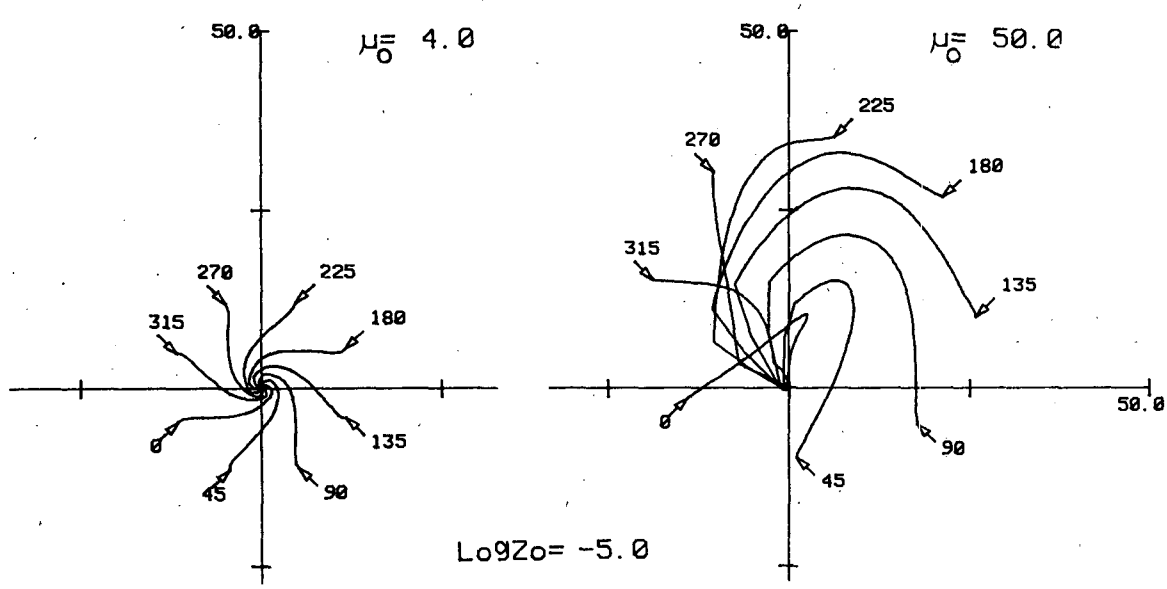

FIG. 7. The hodographs of the dimensionless velocity defects $\kappa u'/u_*$, $\kappa v'/u_*$ for two stabilities $\mu_0 = 4$ and 50. The numbers refer to the angle δ; $\psi = 0.003$, $s = -1$.

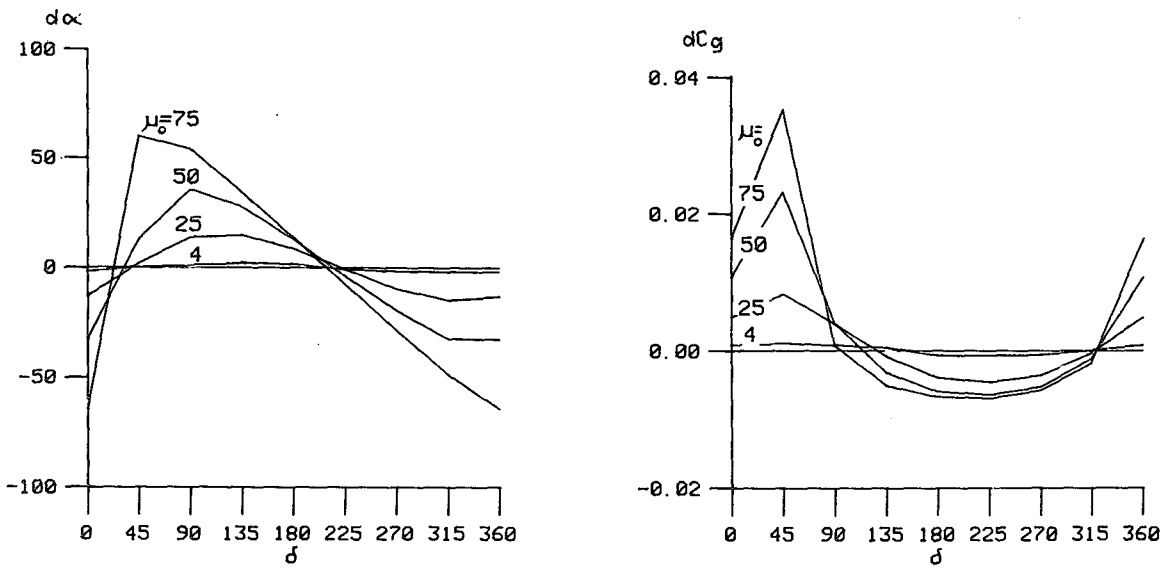

FIG. 8. The slope-caused deviations of the cross-isobar angle α and the geostrophic drag coefficient c_g, from their horizontal values, for different stabilities; $\psi = 0.003$, $Z_0 = 10^{-5}$, $s = -1$.

and turbulence is continuous. The existence of such a range needs an experimental confirmation.

The second effect is due to the inertial oscillations of the wind velocity about its equilibrium value in the free atmosphere. Some influences of these oscillations can be transmitted into the ABL by the entrainment

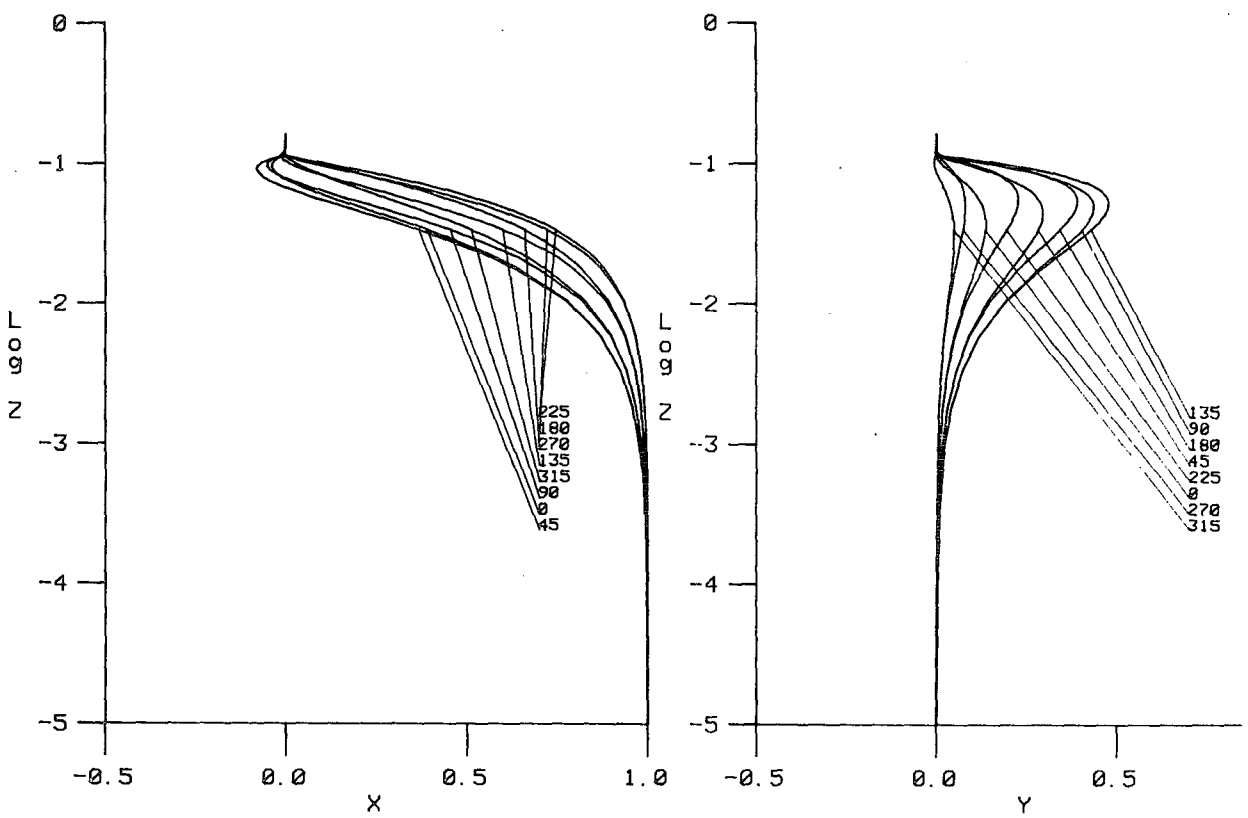

FIG. 9. The dimensionless Reynolds stress vector components X and Y for different values of the angle δ (x-axis along the surface stress vector), $\mu_0 = 50$, $\psi = 0.003$, $s = -1$.

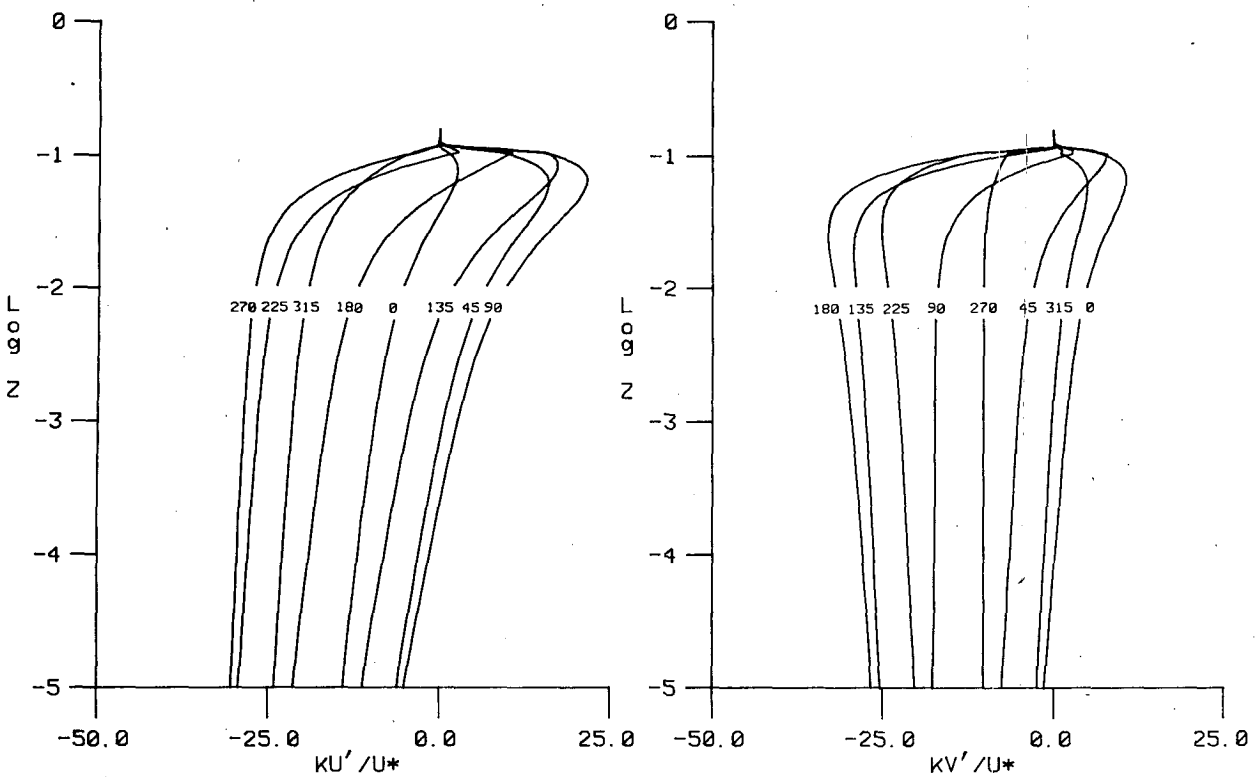

FIG. 10. Dimensionless velocity defect profiles for different values of the angle δ (x-axis along the surface stress vector), $\mu_0 = 50$, $\psi = 0.003$, $s = -1$.

process and can somewhat distort the air flow. However, this effect should not be large in our case, since the entrainment is expected to be weak.

In the stable boundary layer we can also expect the presence of another effect, due to the local generation of turbulence by wave motion. Our model does not predict the local structure and its results should be understood as averaged over an ensemble or over a large, horizontally homogeneous, inclined plane.

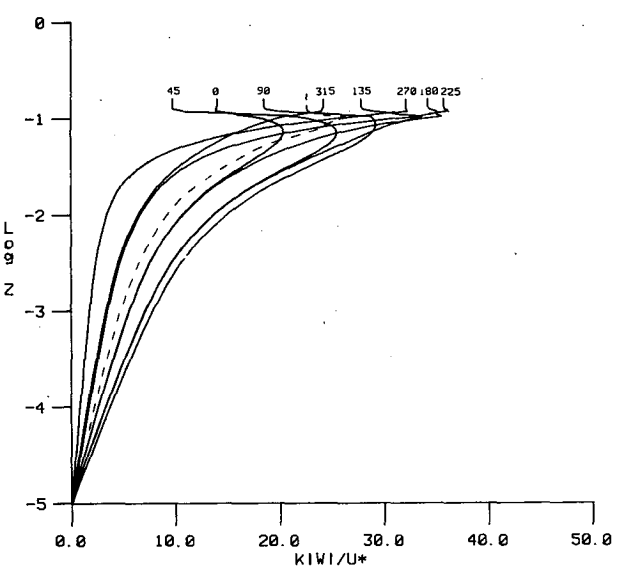

FIG. 11. The dimensionless wind velocity modulus for different values of the angle δ. The dashed curve was obtained for $\psi = 0$ ($s = -1$, $\mu_0 = 50$, $\psi = 0.003$).

c. *Parametrization of the ABL over a slightly inclined terrain*

Numerical models are useful and, in many cases, the one way to obtain detailed and accurate description of complex flows. However, they must be resimulated whenever the set of governing parameters has to be changed. An alternative and cheaper method is the Rossby-number similarity theory. The extension of this theory for the case of a sloping terrain was proposed in S83. It was found that the internal ABL characteristics can be found by the solution of resistance laws in the form

$$\left.\begin{aligned} -\cos\delta \ln(\kappa Z_0) - \kappa \frac{\cos\chi}{c_g} &= A_s \\ \left(s \sin\delta - \frac{\eta}{\alpha_H^0}\right) \ln(\kappa Z_0) + s\kappa \frac{\sin\chi}{c_g} + \eta \frac{\theta_0'}{T_*} &= -B_s \\ \alpha_H^0 \frac{\theta_0'}{T_*} - \ln(\kappa Z_0) &= C_s \end{aligned}\right\}. \tag{16}$$

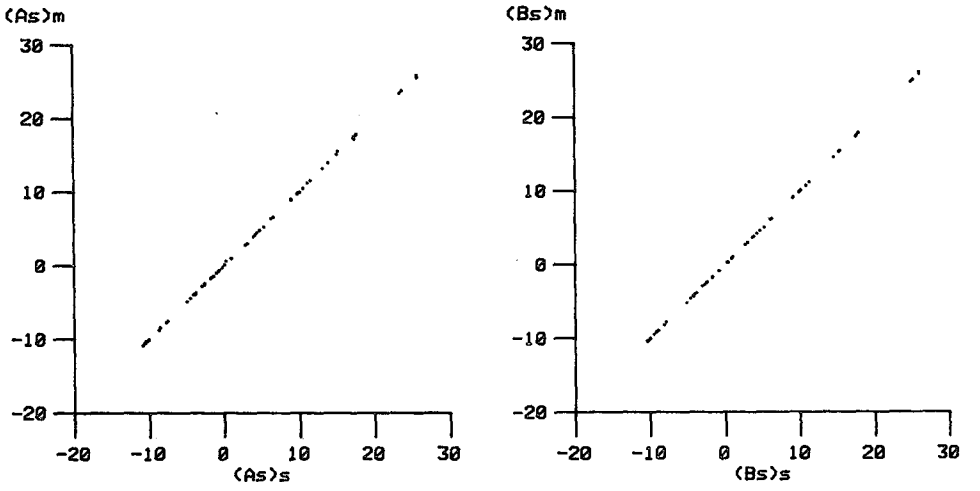

FIG. 12. The comparison of the similarity functions obtained from the model $(A_s)_m$, $(B_s)_m$ [Eq. (14)], with those obtained from the similarity prediction $(A_s)_s$, $(B_s)_s$ [Eq. (17)]. (Points were obtained for all considered stabilities and values of the angle δ.)

The similarity functions A_s, B_s, C_s are the combinations of the similarity functions A, B, C for the horizontal case

$$\left.\begin{aligned} A_s &= A\cos\delta - \left(s\sin\delta - \frac{\eta}{\alpha_H^0}\right)B - \frac{\eta}{\alpha_H^0 Z_T} \\ B_s &= B\cos\delta + \left(s\sin\delta - \frac{\eta}{\alpha_H^0}\right)A \\ C_s &= C \end{aligned}\right\}. \quad (17)$$

In order to demonstrate the validity of these formulas, the present model was used. The resultant functions $(A_s)_m$, $(B_s)_m$ obtained from Eq. (14) versus functions $(A_s)_s$, $(B_s)_s$ computed from the similarity prediction [Eq. (17)] are given in Fig. 12. The model confirms perfectly the similarity prediction, with Z_T described in Eq. (8). In our previous paper (S83), for the sake of simplicity, we assumed that $Z_T = 1$, which cannot be accepted now. The third similarity function C and the heat transfer equation have the same form as for horizontal case.

Empirical determination of the stability-dependent similarity functions of the resistance laws usually results in a large scatter of data points (Zilitinkevich and Chalikov, 1968; Clarke and Hess, 1974; Melgarejo and Deardorff, 1974; Arya, 1975; Yamada, 1976). Some of it, of course, is due to uncertainties in the mea-

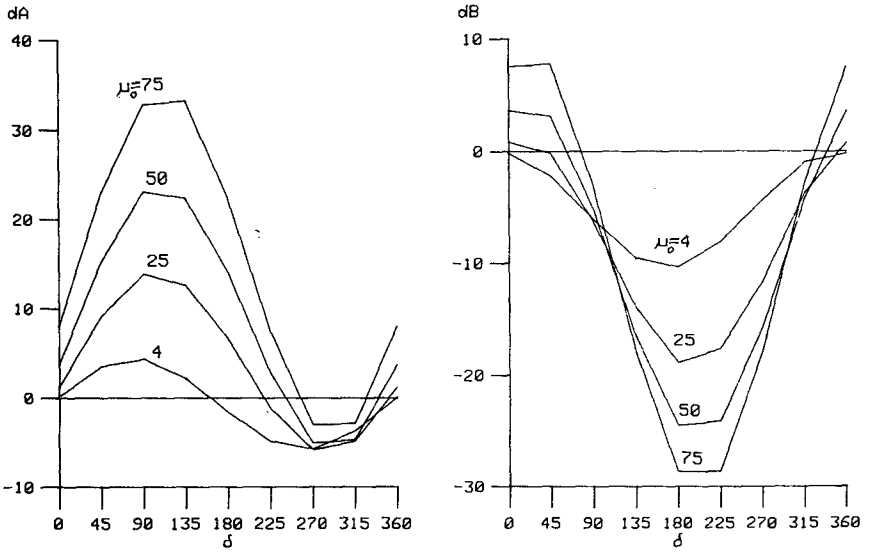

FIG. 13. The slope-caused deviations of the similarity functions from their horizontal values, for different stabilities and different values of the angle δ; $\psi = 0.003$.

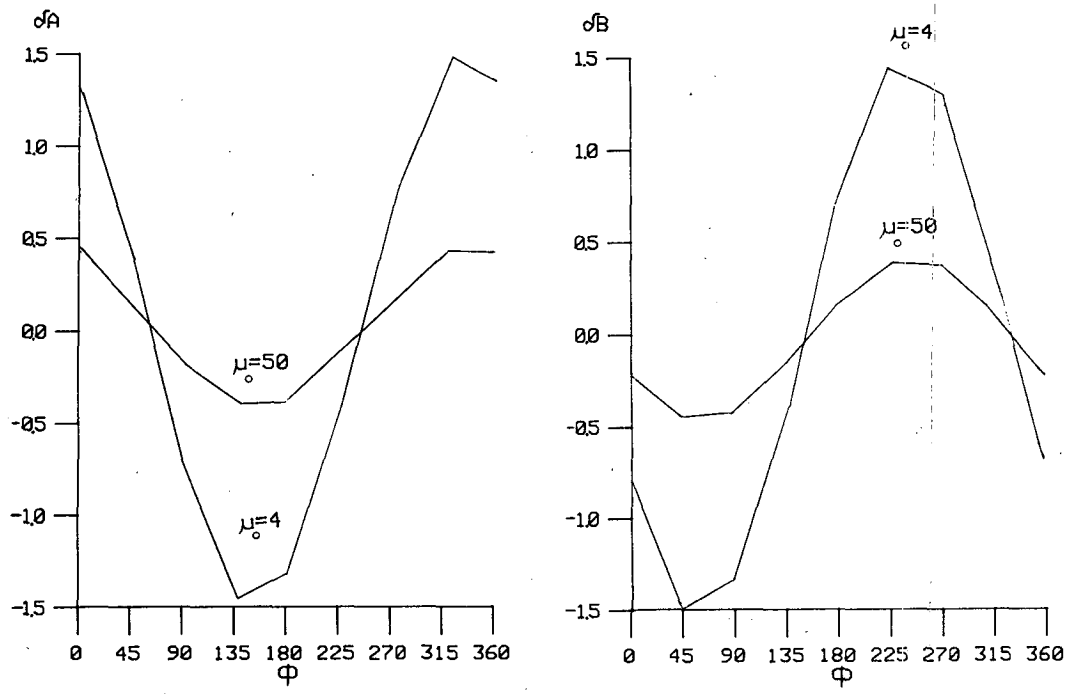

FIG. 14. The differences between baroclinic and barotropic values of similarity functions, for two stabilities $\mu_0 = 4$ and 50 and for different values of the angle δ; $s = -1$, $M = 10$.

surements of the geostrophic wind and the surface fluxes. We hypothesize here that a large part of the scatter is caused by the influence of a sloping terrain.

Some theoretical evidence of that fact is presented in Fig. 13. Here, dA and dB, representing the deviations of similarity functions A_s, B_s from their horizontal values, are shown to be oscillating functions of the angle δ and increasing functions of stability.

In S83b, dealing with the baroclinic case, we deduced that for the weak baroclinicity, the deviations δA, δB of similarity functions A_s, B_s from their barotropic values are the linear functions of the thermal wind components and independent of a slope. They can be expressed as

$$\left.\begin{aligned}\delta A &= aM\cos(s\phi - \phi_a)\\ \delta B &= bM\sin(s\phi - \phi_b)\end{aligned}\right\}, \qquad (18)$$

where a and b are the functions of stability. Our model confirms this prediction. Functions δA and δB, obtained from the model for $\mu_0 = 4$ and 50, are periodic, as shown in Fig. 14. According to our results, ϕ_a and ϕ_b are in the range (0–45°), close to the value 30°, obtained by Wippermann (1972). It can be seen from the figure that in the thin stable ABL, the effect of weak baroclinicity is much smaller than that caused by a slope.

All figures presented in our paper were expressed in terms of the internal stability parameter μ_0. Finally, in Fig. 15, we demonstrate the relation between the internal μ_0 and external σ.

4. Conclusions

The present study was undertaken to examine the Rossby-number similarity over a slightly inclined ter-

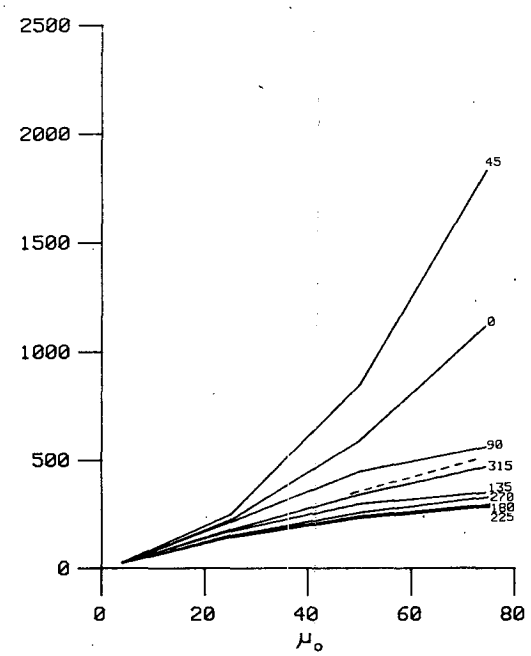

FIG. 15. The relation between the internal μ_0 and the external σ stability parameters for different values of the angle δ. The dashed line was obtained for $\psi = 0$ ($s = -1$, $Z_0 = 10^{-5}$, $\psi = 0.003$).

rain. For this purpose, we considered a simple steady-state model of the stable boundary layer.

It was shown that the similarity profiles of the Reynolds stress components and the wind velocity defects depend strongly on the slope. The slope-dependent parts of similarity functions A_s, B_s were shown to be periodic functions of the angle δ, between the downward slope direction and the surface stress vector, with the amplitudes increasing with stability. The surface cross-isobar angle α and the geostrophic drag coefficient c_g were also found to be oscillating functions of δ.

The model simulation confirms the form of similarity functions predicted by Sorbjan (1983a,b).

On the basis of obtained results, we hypothesized that the large scatter of the similarity functions, reported in the literature, can be explained by the influence of an inclined terrain.

Acknowledgments. This research was completed during the author's short visit to the Geophysical Institute (G.I.) at the University of Alaska in Fairbanks, in the summer of 1983. The author would like to thank Dr. Gerd Wendler (G.I.) for his kind support. Our thanks are also extended to Dr. Uwe Radok (CIRES, Boulder), Dr. Keith Mather (Vice Chancelor for Research, UAF) and Dr. Gunter Weller (Assistant Director, G.I.) for all arrangements connected with my visit. The author would like finally to express his appreciation to Mr. Yuji Kodama for plotting all the figures on the VAX plotter.

The financial support of the National Science Foundation under Grant DPP 8100161 is also acknowledged.

APPENDIX

List of Symbols

A_s, B_s, C_s	universal functions of the sloping terrain resistance laws
A, B, C	universal functions for the horizontal case
c_g	geostrophic drag coefficient
f	modulus of the Coriolis parameter
G	modulus of the geostrophic wind vector
H	dimensionless turbulent heat flux
k	eddy diffusivity
L_*	Monin-Obukhov length
L_E	Ekman length
M	dimensionless modulus of the thermal wind
Q_0	surface heat flux
Ro	surface Rossby number
s	sign of the Coriolis parameter
T_*	temperature scale
u, v	components of the wind velocity vector
U_g, V_g	components of the geostrophic wind vector
u_*	friction velocity
x, z	downslope and normal axis of the terrain-following Cartesian coordinates
X, Y	dimensionless momentum fluxes
Z_0	dimensionless roughness parameter
Z_T	dimensionless height of the ABL
α	angle between the geostrophic wind vector and the surface stress vector
α_H^0	inverse turbulent Prandtl number
β	buoyancy parameter $[=g/T_0]$
δ	angle between the surface stress vector and the x-axis
κ	von Kàrmàn constant
η	parameter $[=\mu_0\psi/\kappa^2]$
η_x, η_y	components of the dimensionless thermal wind
θ, θ_F	potential temperature in the ABL and in the free atmosphere
μ_0	internal stability parameter
σ	external stability parameter
ϕ	angle between the thermal wind vector and the x-axis
χ	angle between the geostrophic wind vector and the x-axis
ψ	slope inclination.

The primes denote the deviations of the boundary layer parameters from the free atmosphere values. The capital letters denote the dimensionless parameters.

REFERENCES

André, J. C., and L. Mahrt, 1982: The nocturnal surface inversion and influence of clear-air radiative cooling. *J. Atmos. Sci.*, **39**, 864–878.

Arya, S. P. S., 1975: Geostrophic drag and heat transfer relations for the atmospheric boundary layer. *Quart. J. Roy. Meteor. Soc.*, **101**, 147–161.

Brost, R. A., and J. C. Wyngaard, 1978: A model study of the stably stratified planetary boundary layer. *J. Atmos. Sci.*, **35**, 1427–1440.

Businger, J. A., and S. P. S. Arya, 1974: Height of the mixed layer in the stably stratified planetary boundary layer. *Advances in Geophysics*, Vol. 18A, Academic Press, 73–92.

——, J. C. Wyngaard, Y. Izumi and F. Brodley, 1971: Flux profile relationship in the atmospheric surface layer. *J. Atmos. Sci.*, **28**, 181–189.

Clarke, R. H., and G. H. Hess, 1974: Geostrophic departure and the functions A and B of Rossby-number similarity theory. *Bound.-Layer Meteor.*, **7**, 267–287.

Gutman, L. N., and J. W. Melgarejo, 1981: On the laws of geostrophic drag and heat transfer over a slightly inclined terrain. *J. Atmos. Sci.*, **38**, 1714–1724.

Kuhn, M., H. H. Lettau and A. J. Riordan, 1977: Stability-related wind spiraling in the lowest 32 meters. *Meteorological Studies at Platau Station, Antarctica*, Antarctic Res. Ser., Vol. 25, Paper 6, 93–111.

Lettau, H. H., 1983: Thoughts on priorities in boundary-layer research. *Bound.-Layer Meteor.*, **25**, 429–432.

——, and A. J. Riordan, 1977: Air temperature and two-dimensional wind profiles in the lowest 32 meters as a function of bulk stability. *Meteorological Studies at Platau Station, Antarctica*, Antarctic Res. Ser., Vol. 25, Paper 6, 77–111.

Mahrt, L. J., and W. S. Schwerdtfeger, 1970: Ekman spirals for exponential thermal wind. *Bound.-Layer Meteor.*, **1**, 137–145.

Melgarejo, J. W., and J. W. Deardorff, 1974: Stability functions for the boundary-layer resistance laws based upon observed boundary-layer heights. *J. Atmos. Sci.*, **31**, 1324–1333.

Sorbjan, Z., 1983a: Rossby-number similarity in the atmospheric boundary layer over a slightly inclined terrain. *J. Atmos. Sci.*, **40**, 718–728.

——, 1983b: Effects of baroclinicity on resistance laws for the atmospheric boundary layer over a slightly inclined terrain. *J. Atmos. Sci.*, **40**, 729–737.

Turner, J. S., 1973: *Buoyancy Effects in Fluids.* Cambridge University Press, 367 pp.

du Vachat, R., and L. Musson-Genon, 1982: Rossby similarity and turbulent formulation. *Bound.-Layer Meteor.*, **23**, 47–68.

Wendler, G., and Y. Kodama, 1983: On the climate of Dome C, Antarctica, in relation to its geographical setting. Submitted to *J. Climatol.*

Wippermann, F., 1972: Baroclinic effects on the resistance law for the planetary boundary layer of the atmosphere. *Beitr. Phys. Atmos.*, **45**, 244–259.

Wyngaard, J. C., 1975: Modeling the planetary boundary layer—extension to the stable case. *Bound.-Layer Meteor.*, **9**, 441–460.

Yamada, T., 1976: On the similarity functions *A*, *B* and *C* of the planetary boundary layer. *J. Atmos. Sci.*, **33**, 781–793.

Yokoyama, O., M. Gamo and S. Yamamoto, 1979: The vertical profiles of the turbulence quantities in the atmospheric boundary layer. *J. Meteor. Soc. Japan*, **3**, 265–272.

Zilitinkevich, S. S., 1972: On the determination of the height of the Ekman boundary layer. *Bound.-Layer Meteor.*, **3**, 141–145.

——, 1975: Resistance laws and prediction equations for the depth of the planetary boundary layer. *J. Atmos. Sci.*, **32**, 741–753.

——, and D. V. Chalikov, 1968: The laws of resistance and of heat and moisture exchange in the interaction between the atmosphere and an underlying surface. *Izv. Acad. Sci. USSR, Atmos. Ocean Phys.*, **4**, 438–441.